The Astrophysical Journal, 740:75 (7pp), 2011 October 20 doi:10.1088/0004-637X/740/2/75


# EVOLUTION OF SUPER STAR CLUSTER WINDS WITH STRONG COOLING

Richard Wünsch[1], Sergiy Silich[2], Jan Palouš[1], Guillermo Tenorio-Tagle[2], and Casiana Muñoz-Tuñón[3,4]
[1] Astronomical Institute, Academy of Sciences of the Czech Republic, Boční II 1401, 141 31 Prague, Czech Republic
[2] Instituto Nacional de Astrofísica Optica y Electrónica, AP 51, 72000 Puebla, Mexico
[3] Instituto de Astrofísica de Canarias, c/ Vía Láctea s/n, E-38205 La Laguna, Tenerife, Spain
[4] Departamento de Astrofisica, Universidad de La Laguna, E-38205 La Laguna, Tenerife, Spain
*Received 2011 May 6; accepted 2011 July 25; published 2011 September 30*

## ABSTRACT

We study the evolution of super star cluster winds driven by stellar winds and supernova explosions. Time-dependent rates at which mass and energy are deposited into the cluster volume, as well as the time-dependent chemical composition of the re-inserted gas, are obtained from the population synthesis code Starburst99. These results are used as input for a semi-analytic code which determines the hydrodynamic properties of the cluster wind as a function of cluster age. Two types of winds are detected in the calculations. For the quasi-adiabatic solution, all of the inserted gas leaves the cluster in the form of a stationary wind. For the bimodal solution, some of the inserted gas becomes thermally unstable and forms dense warm clumps which accumulate inside the cluster. We calculate the evolution of the wind velocity and energy flux and integrate the amount of accumulated mass for clusters of different mass, radius, and initial metallicity. We also consider conditions with low heating efficiency of the re-inserted gas or mass loading of the hot thermalized plasma with the gas left over from star formation. We find that the bimodal regime and the related mass accumulation occur if at least one of the two conditions above is fulfilled.

*Key words:* galaxies: star clusters: general – H II regions – ISM: bubbles – ISM: general

*Online-only material:* color figure

## 1. INTRODUCTION

Super star clusters (SSCs) are young compact objects observed in many starburst and interacting galaxies in a variety of wavelengths (Holtzman et al. 1992; Whitmore et al. 1993; O'Connell et al. 1995; Melo et al. 2005; Smith et al. 2006; Gilbert & Graham 2007; Galliano et al. 2008; Whelan et al. 2011). With masses $10^5$–$10^7\,M_\odot$ and ages $\lesssim 10^7$ yr they are expected to include large numbers of massive stars which lose substantial fractions of their mass via stellar winds and supernova (SN) explosions.

Chevalier & Clegg (1985, hereafter CC85) studied the hydrodynamics of the gas re-inserted by massive stars into the cluster interior using an adiabatic spherically symmetric model. They assumed that the mechanical energy of stellar winds and SNe ejecta is thermalized in random collisions and the gas within the cluster is heated up to $\sim 10^7$ K. The resulting high pressure drives the cluster wind for which CC85 found a stationary hydrodynamic solution. They assumed that the mass and the thermal energy are inserted uniformly at rates $\dot{M}_{\rm SC}$ and $L_{\rm SC}$, respectively, into a sphere (cluster) of radius $R_{\rm SC}$. They showed that, under such assumptions, a stationary wind can only be obtained if the flow velocity equals zero at the cluster center and reaches the sound speed exactly at the cluster border. SSC winds were studied further using analytical and numerical models by many authors including Cantó et al. (2000), Raga et al. (2001), Silich et al. (2003), and Tenorio-Tagle et al. (2006).

It was found by Silich et al. (2004) that the adiabatic approximation becomes inadequate for very massive and compact clusters. The authors showed that the stationary solution of the cluster wind does not exist for clusters with $L_{\rm SC}$ larger than a critical value $L_{\rm crit}$. This is because the total energy input rate, $L_{\rm SC}$, is proportional to the cluster stellar mass, $M_\star$, while the energy losses from the hot gas due to radiation are proportional to $M_\star^2$ (since cooling is proportional to the second power of the gas density which is proportional to $M_\star$). Silich et al. (2004) showed how $L_{\rm crit}$ depends on the star cluster parameters and Wünsch et al. (2007) found an approximate analytical formula for $L_{\rm crit}$.

Clusters with $L_{\rm SC} > L_{\rm crit}$ were studied by means of one-dimensional hydrodynamic simulations by Tenorio-Tagle et al. (2007), who showed that such clusters evolve in the bimodal hydrodynamic regime. In such a case, the cluster is divided by the stagnation radius, $R_{\rm st}$, into two qualitatively different regions. The stationary wind solution still exists in the outer region $r > R_{\rm st}$, with the wind velocity being zero at $R_{\rm st}$ and reaching the sound speed at $R_{\rm SC}$. In the region $r < R_{\rm st}$, on the other hand, the thermal instability sets in and random parcels of gas cool down to $\sim 10^4$ K (further cooling is prevented by the intense stellar radiation). Consequently, the warm regions are compressed into dense clumps by repressurizing shocks driven by the surrounding hot gas. Clusters in the bimodal regime were studied further by Wünsch et al. (2008) who used two-dimensional hydrodynamics to follow the clump formation, and to estimate the fraction of the re-inserted matter which leaves the cluster as a wind and the fraction which accumulates inside the stagnation radius and possibly leads to secondary star formation (Tenorio-Tagle et al. 2005).

It was suggested that two-component supersonic recombination line profiles often detected in young and massive SSCs (Gilbert & Graham 2007; Beck 2008; Henry et al. 2007) and compact dense H II regions overlapping young SSCs (Smith et al. 2006) may present the observational manifestation for such a bimodal regime (Tenorio-Tagle et al. 2010; Silich et al. 2007, 2009). In both cases the calculations require the shocked gas temperature to be lower than that predicted by the CC85 model as is also the case when the model-predicted diffuse X-ray emission is compared to the observed values (Stevens & Hartwell 2003). Two different processes which may decrease the intercluster gas temperature have been discussed in the

literature: the efficiency with which the kinetic energy of stellar winds and SNe is thermalized, and the additional mass loading into the hot gas inside the cluster (Stevens & Hartwell 2003; Melioli & de Gouveia Dal Pino 2004; Wünsch et al. 2007; Silich et al. 2007, 2009, 2010). In this work we do not discuss details related to those two processes; however, we introduce two free parameters $\eta_{\rm he}$ and $\eta_{\rm ml}$ and show how the results depend on their values.

Previous works on clusters in the bimodal regime use the energy and mass deposition rates $L_{\rm SC}$ and $\dot{M}_{\rm SC}$ as free parameters. In this work, we calculate time-dependent $L_{\rm SC}(t)$ and $\dot{M}_{\rm SC}(t)$ using the stellar population synthesis code Starburst99 (Leitherer et al. 1999) for a cluster with a given stellar mass, $M_\star$, and initial stellar metallicity, $Z_0$. Subsequently, we insert $L_{\rm SC}(t)$ and $\dot{M}_{\rm SC}(t)$ into our semi-analytic code to determine the evolutionary properties of the cluster wind. We also calculate whether the cluster spends some time in the bimodal regime and estimate the amount of re-inserted gas which becomes thermally unstable and accumulates inside the cluster. The Starburst99 code also provides us with the time evolution of the chemical composition of the re-inserted gas. The chemical composition is an important parameter as the cooling rate depends on it. This work effectively replaces the three functions of time, $L_{\rm SC}(t)$, $\dot{M}_{\rm SC}(t)$, and $Z(t)$ (metallicity of the cluster wind), with two constant parameters: the mass of the star cluster $M_\star$ and its initial metallicity $Z_0$.

The paper is organized as follows: in Section 2 we describe the semi-analytic code used for the calculation of the cluster wind and the way in which it utilizes the results of the Starburst99 code. In Section 3, we show results for a reference model with $M_\star = 10^6\,M_\odot$ and $R_{\rm SC} = 3$ pc (Section 3.1) and give the dependence of these results on the cluster mass, the cluster radius, and the initial stellar metallicity (Section 3.2). In Section 4 we summarize our conclusions.

## 2. THE CLUSTER WIND

In this section, we specify the assumptions used in the semi-analytic model of the cluster wind and formulate its basic equations. We also describe how the model equations are integrated and the properties of the bimodal solution (e.g., $R_{\rm st}$, $L_{\rm crit}$, and $\dot{M}_{\rm wind}$) determined. Finally, we describe how the wind model utilizes the output from the Starburst99 code.

### 2.1. Assumptions and Basic Equations

We consider a spherical cluster of radius $R_{\rm SC}$ whose stars deposit mass and energy at rates $\dot{M}_{\rm SC}$ and $L_{\rm SC}$, respectively. We assume, similar to CC85, that mutual collisions of stellar winds and SNe ejecta, and collisions with gas left over from the formation of the first stellar generation and with gas returned by pre-main-sequence stars via outflows, result in the production of hot gas which occupies most of the cluster volume. Therefore, we model these processes by inserting mass and energy uniformly into the whole cluster volume with deposition rate densities $q_m$ and $q_e$. In order to account for the uncertainties related to the thermalization of the mechanical energy of the inserted gas we introduce the heating efficiency, $\eta_{\rm he} \in (0, 1)$, denoting the fraction of the mechanical energy of stellar winds and SNe ejecta which is converted into the thermal energy of the hot gas. Furthermore, we assume that a substantial amount of gas was left over after the formation of the first generation of stars and that this gas may evaporate and be dispersed into the hot gas. Another contribution to the mass of hot gas inside the cluster comes from outflows of pre-main-sequence stars which are not included in the Starburst99 code. Indeed, the mass left over from star formation and the T Tauri multiple outflows, such as the jet from RW Aurigae (Bacciotti et al. 1996), should make a substantial contribution to the mass available for mass loading. We describe these processes by the mass loading factor, $\eta_{\rm ml} \in (0, \infty)$, which gives the amount of the loaded mass relative to $\dot{M}_{\rm SC}$. The total mass injection rate then is $\dot{M}_{\rm in} = \dot{M}_{\rm SC} + \eta_{\rm ml}\dot{M}_{\rm SC} = (1 + \eta_{\rm ml})\dot{M}_{\rm SC}$. It is assumed that the metallicity of the loaded gas is the same as the initial stellar metallicity, $Z_0$.

The spherically symmetric hydrodynamic equations describing the wind flow are (CC85; Silich et al. 2004)

$$\frac{1}{r^2}\frac{d}{dr}(\rho u r^2) = q_m \tag{1}$$

$$\rho u \frac{du}{dr} = -\frac{dP}{dr} - q_m u \tag{2}$$

$$\frac{1}{r^2}\frac{d}{dr}\left[\rho u r^2 \left(\frac{u^2}{2} + \frac{\gamma}{\gamma - 1}\frac{P}{\rho}\right)\right] = q_e - Q, \tag{3}$$

where $\gamma$ is the adiabatic index and $\rho$, $u$, and $P$ are wind density, velocity, and pressure, respectively. Mass and energy deposition rate densities $q_m$ and $q_e$ are

$$\begin{aligned} q_m &= \frac{3(1+\eta_{\rm ml})\dot{M}_{\rm SC}}{4\pi R_{\rm SC}^3} \\ q_e &= \frac{3\eta_{\rm he} L_{\rm SC}}{4\pi R_{\rm SC}^3} \end{aligned} \tag{4}$$

for $r < R_{\rm SC}$ and $q_m = q_e = 0$ for $r > R_{\rm SC}$. The energy equation (3) includes the cooling term $Q = n_i n_e \Lambda(T, Z)$ where $n_i = n_e = \rho/\mu_i$ are the ion and electron number densities, $Z$ is the gas metallicity, and $\Lambda(T, Z)$ is a cooling function tabulated by Plewa (1995). We use $\mu_i = 14/11 m_{\rm H}$ neglecting the contribution of heavy elements.

Several interesting properties may be derived directly from Equations (1)–(3) (see Silich et al. 2004 for details). First, the stationary solution exists only if the wind velocity, $u$, reaches the sound speed exactly at the cluster border. Second, a relation between the temperature $T_{\rm st}$ and the density $\rho_{\rm st}$ at the stagnation radius can be derived:

$$\rho_{\rm st} = \left[\frac{q_e - q_m c_{\rm st}^2/(\gamma - 1)}{\Lambda(T_{\rm st}, Z)}\right]^{1/2}, \tag{5}$$

where $c_{\rm st}$ is the sound speed at the stagnation radius. Furthermore, it has been shown by Tenorio-Tagle et al. (2007) that if the cluster is in the bimodal regime, i.e., if $R_{\rm st} > 0$, the pressure at the stagnation radius $P_{\rm st} = (k\rho_{\rm st}T_{\rm st})/\mu_a$ reaches the maximum value $P_{\rm max} = \max(P_{\rm st}(T_{\rm st}))$, where $k$ denotes the Boltzmann constant and $\mu_a = 14/23 m_{\rm H}$ is the mean mass per particle.

### 2.2. Integration Procedure

The wind solution is found by the following procedure. At first, it is assumed that $R_{\rm st} = 0$ and an attempt to find $T_{\rm st}$ is made. Equations (1)–(3) are repeatedly integrated numerically from $r = 0$ to $R_{\rm SC}$ with $T_{\rm st}$ varying in the interval $(0, T_a)$ where $T_a = (\gamma - 1)\mu_a q_e/(\gamma k q_m)$ is the adiabatic wind central temperature. The central density $\rho_{\rm st}$ is calculated from Equation (5). Then, the

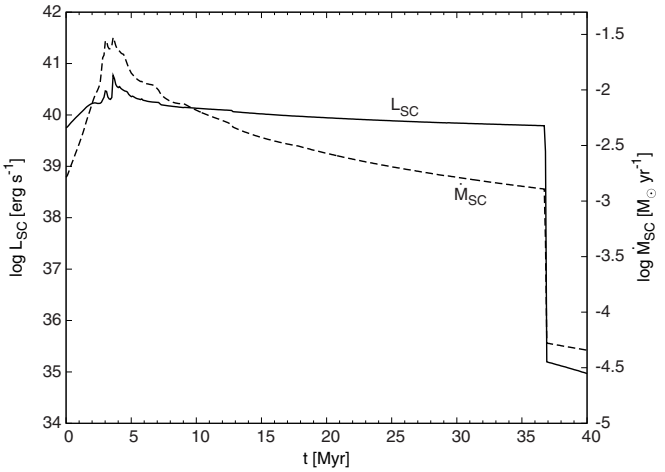


**Figure 1.** Energy (solid line, left $y$-axis) and mass (dashed line, right $y$-axis) deposition rates calculated by the Starburst99 code for the reference model $M_\star = 10^6\,M_\odot$, $R_{SC} = 3$ pc, $Z_0 = Z_\odot$, $\eta_{he} = 1$, and $\eta_{ml} = 0$.

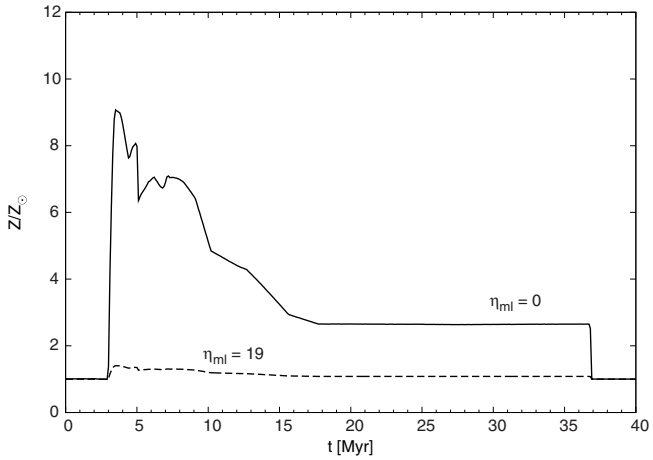


**Figure 2.** Evolution of the metallicity of the hot shocked gas inside the cluster with $Z_0 = Z_\odot$. The solid and dashed lines show the metallicity without ($\eta_{ml} = 0$) and with ($\eta_{ml} = 19$) mass loading, respectively.

bisection method is used to find $T_{st}$ for which the sonic radius $R_{son}$ (defined as $u(R_{son}) = c_s(R_{son})$) is equal to $R_{SC}$.

If this attempt fails (i.e., no initial conditions at $r = 0$ for which $R_{son} = R_{SC}$ exist), it implies that $R_{st} > 0$ and the cluster is in the bimodal regime. In such a case, the value of $T_{st}$ is defined by the condition that the function $P_{st}(T_{st})$ has its maximum $P_{max}$ (Tenorio-Tagle et al. 2007). Therefore, the temperature at the stagnation radius is found using the golden section method and it is used as the initial condition for integrating Equations (1)–(3). Then, similarly to the previous case, $R_{st}$ is varied and the bisection method is used to find the solution which satisfies the condition $R_{son} = R_{SC}$.

Once all the initial conditions ($R_{st}$, $\rho_{st}$, and $T_{st}$) are known, radial profiles of the wind density $\rho$, velocity $u$, and temperature $T$ can be obtained by integrating Equations (1)–(3) in the interval ($R_{st}$, 10 $R_{SC}$). The semi-analytic model is unable to describe the inner thermally unstable region with $r < R_{st}$. However, two-dimensional hydrodynamic simulations (Wünsch et al. 2008) have shown that the temperature and the density of the hot gas in this region are close to uniform and stay constant with time. The deposition of mass into this region is balanced by the formation of dense warm clumps which tend to accumulate in this region. Therefore, we assume that the hot gas in the central region $r < R_{st}$ has zero velocity, uniform density $\rho_{st}$, and temperature $T_{st}$, and that all gas inserted into this region accumulates there. Finally, the critical luminosity $L_{crit}$ is determined by repeating the above procedure and searching for the lowest mechanical luminosity $L_{SC}$ for which $R_{st} > 0$.

### 2.3. Starburst99 Outputs Used in the Wind Model

The stellar population synthesis code Starburst99 (Leitherer et al. 1999) calculates a set of stellar evolution models for a given population of stars and determines their collective properties. In this work, the total mass-loss rate from stellar winds and SNe type II ejecta is used as the mass deposition rate, $\dot{M}_{SC}$, and the total stellar wind and SNe ejecta power as the energy deposition rate, $L_{SC}$. All Starburst99 simulations used in this work are set up with the following parameters: star formation is instantaneous with the fixed stellar mass $M_\star$; the standard Kroupa initial mass function (IMF; Kroupa 2001) with two power laws ($dN/dm \sim m^{-1.3}$ between 0.1 and 0.5 $M_\odot$ and $dN/dm \sim m^{-2.3}$ between 0.5 and 100 $M_\odot$) is used; the SN cutoff mass is equal to 8 $M_\odot$; stellar evolutionary tracks are Geneva with high mass loss; and the wind model is evolutionary (see Leitherer et al. 1992 for details). The evolution of $\dot{M}_{SC}$ and $L_{SC}$ for the reference model (see Section 3.1) is shown in Figure 1. We have followed the first 40 Myr of the cluster evolution. This period is long enough to cover the lifetime of all massive stars even in cases with initial stellar metallicities, $Z_0$, different than $Z_\odot$, discussed in Section 3.2. We do not consider here the period after the last massive star explodes (this moment is visible as a sudden drop of $\dot{M}_{SC}$ and $L_{SC}$ at 37 Myr in Figure 1).

Starburst99 also provides the chemical composition of the re-inserted matter by specifying mass-loss rates for H, He, C, N, O, Mg, Si, S, and Fe. Thus one can calculate the injection rate for seven elements heavier than H and He:

$$\dot{M}_{metals} = \sum_{j=C}^{Fe} \dot{M}_j, \qquad (6)$$

where $\dot{M}_j$ is the mass deposition rate of the $j$th element. It is assumed that the injected gas is rapidly mixed with the mass-loaded gas. The metallicity of the cluster wind, $Z$, used in Equation (3) is

$$Z = \frac{\dot{M}_{metals} + \eta_{ml} Z_0 \dot{M}_{SC}}{(1 + \eta_{ml})\dot{M}_{SC}}. \qquad (7)$$

The evolution of $Z$ in the cluster with $Z_0 = Z_\odot$ for different values of $\eta_{ml}$ is shown in Figure 2. Taken together, the model utilizing Starburst99 results includes five parameters: $M_\star$, $R_{SC}$, $Z_0$, $\eta_{he}$, and $\eta_{ml}$. The semi-analytic wind model on its own includes six parameters: $\dot{M}_{SC}$, $L_{SC}$, $Z$, $R_{SC}$, $\eta_{he}$, and $\eta_{ml}$. Here we assume that the first three of these ($\dot{M}_{SC}$, $L_{SC}$, $Z$) are functions of the star cluster age. We keep the heating efficiency, $\eta_{he}$, and the mass loading coefficient, $\eta_{ml}$, constant, although they may change with time as the number of massive stars and the amount of gas left over from star formation decrease.

## 3. RESULTS

In the first part of this section (Section 3.1), we describe in detail results for our reference model whose parameters are chosen to represent a typical SSC. Since the heating efficiency, $\eta_{he}$, and the mass loading factor, $\eta_{ml}$, are free parameters, we show results for three different combinations of these. In Section 3.2,

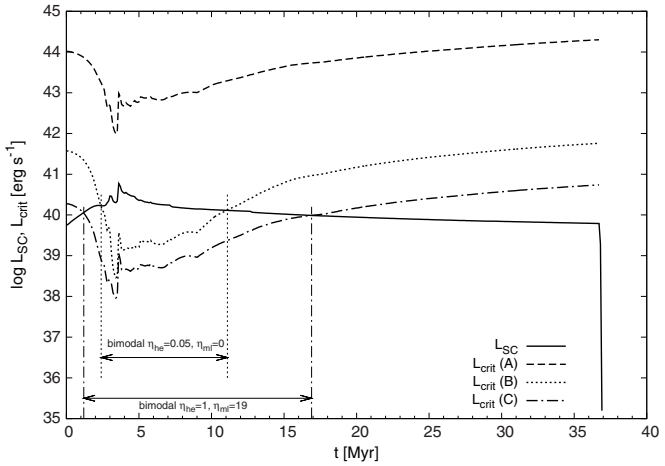


**Figure 3.** Evolution of the critical luminosity, $L_{\rm crit}$, for models A (dashed), B (dotted), and C (dash-dotted). The $L_{\rm crit}$ curves are compared to the cluster mechanical luminosity $L_{\rm SC}$ (solid). Periods during which the cluster evolves in the bimodal regime are denoted by arrows.

**Table 1**
The Reference Model Calculated with Different $\eta_{\rm he}$ and $\eta_{\rm ml}$

| Model | $\eta_{\rm he}$ | $\eta_{\rm ml}$ | $t_{\rm bs}$ (Myr) | $t_{\rm be}$ (Myr) | $M_{\rm acc}$ ($M_\odot$) | $M_{\rm in}$ ($M_\odot$) |
|---|---|---|---|---|---|---|
| A | 1 | 0 | ... | ... | 0 | $1.8 \times 10^5$ |
| B | 0.05 | 0 | 2.4 | 11.1 | $5.8 \times 10^4$ | $1.8 \times 10^5$ |
| C | 1 | 19 | 1.3 | 16.9 | $1.8 \times 10^6$ | $3.7 \times 10^6$ |

**Notes.** Columns 4 and 5 denote the beginning and the end of the period of bimodality ($L_{\rm SC} > L_{\rm crit}$). Columns 6 and 7 show the amount of mass accumulated inside the cluster, $M_{\rm acc}$, and the total amount of mass, $M_{\rm in}$, supplied into the cluster by stars and mass loading, respectively.

we show how the most important results (the existence of the bimodal regime and the amount of the accumulated mass) depend on the cluster mass, the cluster radius, and the initial metallicity of stars and the mass-loaded gas $Z_0$.

### 3.1. The Reference Model

We calculate the evolution of a wind driven by a cluster with a stellar mass $M_\star = 10^6\,M_\odot$, radius $R_{\rm SC} = 3$ pc, and initial stellar metallicity $Z_0 = Z_\odot = 0.02$. We explore three combinations of $\eta_{\rm he}$ and $\eta_{\rm ml}$ (see Table 1). In model A, there is no mass loading and the heating efficiency is 100%. Model B is chosen to be in agreement with Silich et al. (2007, 2009) who obtained $\eta_{\rm he} \simeq 5\%$ in order to fit the parameters of the compact H II regions observed around 11 SSCs selected in the central zone of M82. In model C, the mass loading factor, $\eta_{\rm ml} = 19$, is set to give the same value of $V_{\eta,\infty}$, as in model B, where

$$V_{\eta,\infty} = \left[\frac{2\eta_{\rm he} L_{\rm SC}}{(1+\eta_{\rm ml})\dot{M}_{\rm SC}}\right]^{1/2} \quad (8)$$

is the adiabatic wind terminal speed corrected for effects of heating efficiency and mass loading.

Figure 3 compares the time evolution of the critical luminosity, $L_{\rm crit}$, with the star cluster mechanical luminosity, $L_{\rm SC}$. In model A the star cluster mechanical luminosity is always below the critical value, $L_{\rm SC} < L_{\rm crit}$, and thus all gas re-inserted by stars leaves the cluster as a wind. On the other hand, models B and C present periods with $L_{\rm SC} > L_{\rm crit}$ when clusters evolve in the bimodal regime. The beginning and the end of these periods are shown in Table 1 in columns $t_{\rm bs}$ and $t_{\rm be}$, respectively.

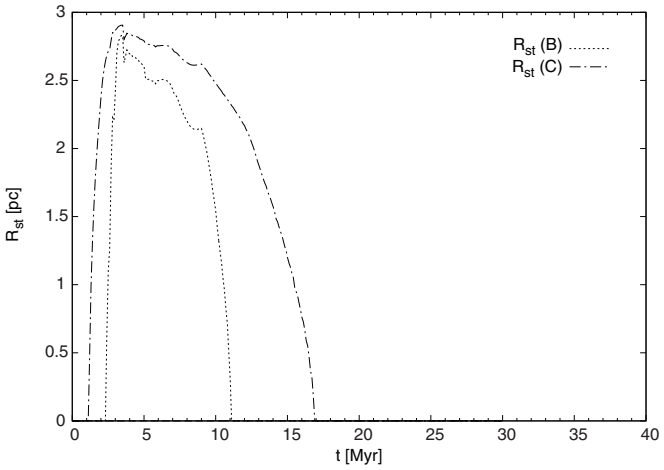


**Figure 4.** Evolution of the stagnation radius, $R_{\rm st}$, for models B (dotted) and C (dash-dotted). The stagnation radius is always zero in model A.

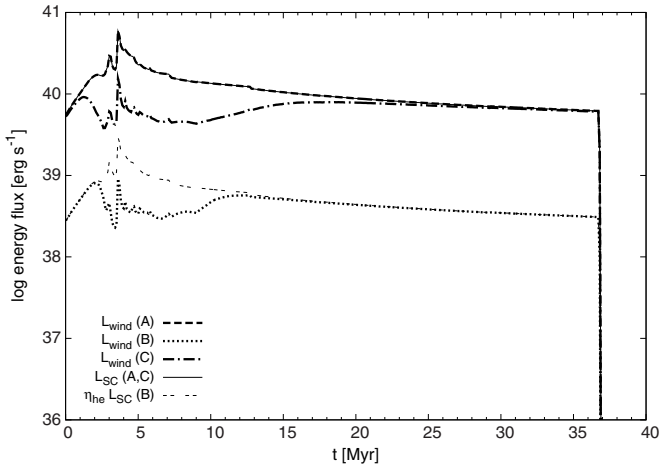


**Figure 5.** Evolution of the wind mechanical output rate, $L_{\rm wind}$, for models A, B, and C is shown by thick dashed, dotted, and dash-dotted lines, respectively. The thin solid curve shows the star cluster mechanical luminosity, $L_{\rm SC}$. It overlaps with the thick dashed curve because, for model A, cooling from the hot wind is negligible and $L_{\rm wind} = L_{\rm SC}$. The thin double-dashed line represents the heating efficiency reduced energy deposition rate, $\eta_{\rm he} L_{\rm SC}$, for model B with $\eta_{\rm he} = 0.05$.

Even though models B and C have the same $V_{\eta,\infty}$, the period of bimodality is longer in model C. This is because, due to mass loading, the density of the thermalized plasma is larger in model C and this results in a higher cooling rate that favors thermal instabilities and mass accumulation.

The stagnation radius, $R_{\rm st}$, for the three models is shown in Figure 4. For model A, it is always at the cluster center, while in the other two cases $R_{\rm st}$ reaches a substantial fraction of $R_{\rm SC}$ when the clusters evolve in the bimodal regime. This implies that the amount of mass accumulated in the central zones of the cluster may be significant if the heating efficiency is low or the mass loading is large. This is because the mass accumulation rate is $\dot{M}_{\rm acc} = \dot{M}_{\rm in}(R_{\rm st}/R_{\rm SC})^3$ where $\dot{M}_{\rm in} = (1+\eta_{\rm ml})\dot{M}_{\rm SC}$ is the rate at which mass is supplied into the cluster by stars and mass loading. For example, the amount of accumulated matter, $M_{\rm acc} = \int_{t_{\rm bs}}^{t_{\rm be}} \dot{M}_{\rm acc} dt$, is about one-third of the total mass supplied into the cluster, $M_{\rm in} = \int_{t_{\rm bs}}^{t_{\rm be}} \dot{M}_{\rm in} dt$, in the case of model B and about one-half of $M_{\rm in}$ in the case of model C (see Table 1).

Note that strong radiative cooling also affects the star cluster wind mechanical output rate, $L_{\rm wind} = 4\pi\rho u r^2(u^2/2+H)$, where $H$ is the enthalpy. Figure 5 shows that in the bimodal regime

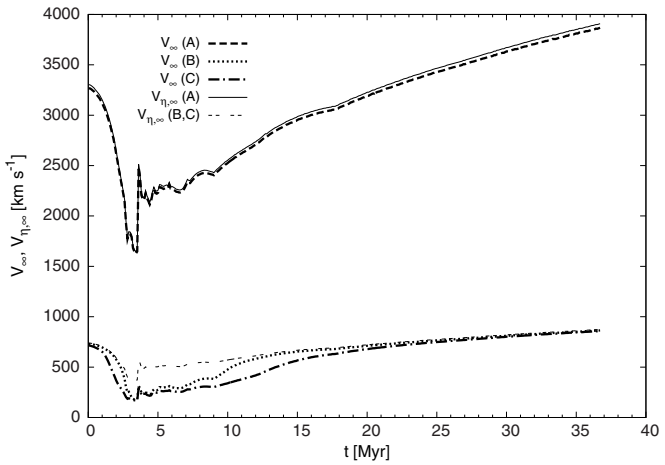


**Figure 6.** Evolution of wind terminal speed, $V_\infty$. Thick dashed, dotted, and dash-dotted lines show the calculated wind terminal speed in the case of models A, B, and C, respectively. Thin lines display $V_{\eta,\infty}$ (see Equation (8)) for model A (solid) and models B and C (double dashed).

it falls well below the star cluster mechanical luminosity, $L_{\rm SC}$ (model C), and below the heating efficiency reduced star cluster mechanical luminosity, $\eta_{\rm he} L_{\rm SC}$ (model B). This implies that the "true" energy output and thus the impact of SSCs on the ambient interstellar medium may be much smaller than one would expect from star cluster synthetic models like Starburst99. Note also that the star cluster wind terminal speed in such cases is smaller than that expected from the star cluster synthetic models (see Figure 6). This figure compares the wind terminal speed $V_\infty$ (measured from semi-analytic models at $r = 10\,R_{\rm SC}$) to the heating efficiency and mass-loading-corrected adiabatic wind terminal speed $V_{\eta,\infty}$. The difference between the two, significant mainly during bimodality periods, is due to radiative energy losses from the wind.

### 3.2. Dependence on the Stellar Cluster Parameters

In this section we explore how our results depend on the cluster parameters running models A, B, and C for clusters with different masses ($M_\star = 10^5$, $10^6$, and $10^7\,M_\odot$), different radii ($R_{\rm SC} = 1$, 3, 10, and 30 pc), and taking into consideration the variation of the re-inserted gas metallicity. The results of the calculations for stellar clusters with different masses and radii when the re-inserted and the ablated gas metallicity were fixed to the solar value are presented in Figure 7. This figure compares the calculated critical mechanical luminosities, $L_{\rm crit}$, to the star cluster mechanical luminosity obtained from the Starburst99 synthetic model. Figure 7 shows that clusters with $\eta_{\rm he} = 1$ and $\eta_{\rm ml} = 0$ never evolve in the bimodal regime. On the other hand, models with low heating efficiency or large mass loading exhibit periods of bimodality (see Tables 2 and 3). In the extreme cases the amount of mass accumulated inside the cluster, $M_{\rm acc}$, may reach 70% of the re-inserted and ablated mass, as is the case when $\eta_{\rm ml} = 19$ and $M_\star = 10^7\,M_\odot$. Note that Wünsch et al. (2007) derived an approximate analytic formula for $L_{\rm crit}$ which predicts that $L_{\rm crit}$ is in direct proportion to the size of the cluster, $R_{\rm SC}$. This is in excellent agreement with our semi-analytic results. Note also that both $L_{\rm SC}$ and $\dot{M}_{\rm SC}$ are linearly proportional to $M_\star$, resulting in $L_{\rm crit}$ independent of $M_\star$. Thus, $L_{\rm crit}$ defines the critical cluster mass, $M_{\rm crit}$, and clusters evolve

**Table 2**
Clusters with Different Stellar Mass, $M_\star$, Heating Efficiency, $\eta_{\rm he}$, and Mass Loading $\eta_{\rm ml}$

| $M_\star$ ($M_\odot$) | $\eta_{\rm he}$ | $\eta_{\rm ml}$ | $t_{\rm bs}$ (Myr) | $t_{\rm be}$ (Myr) | $M_{\rm acc}$ ($M_\odot$) | $M_{\rm in}$ ($M_\odot$) |
|---|---|---|---|---|---|---|
| $10^5$ | 1 | 0 | ... | ... | 0 | $1.8 \times 10^4$ |
| $10^6$ | 1 | 0 | ... | ... | 0 | $1.8 \times 10^5$ |
| $10^7$ | 1 | 0 | ... | ... | 0 | $1.8 \times 10^6$ |
| $10^5$ | 0.05 | 0 | 3.1 | 5.1 | $1.1 \times 10^3$ | $1.8 \times 10^4$ |
| $10^6$ | 0.05 | 0 | 2.4 | 11.1 | $5.8 \times 10^4$ | $1.8 \times 10^5$ |
| $10^7$ | 0.05 | 0 | 1.6 | 17.3 | $1.0 \times 10^6$ | $1.8 \times 10^6$ |
| $10^5$ | 1 | 19 | 2.1 | 9.8 | $8.0 \times 10^4$ | $3.7 \times 10^5$ |
| $10^6$ | 1 | 19 | 1.2 | 16.9 | $1.8 \times 10^6$ | $3.7 \times 10^6$ |
| $10^7$ | 1 | 19 | 0.0 | 36.8 | $2.8 \times 10^7$ | $3.7 \times 10^7$ |

**Notes.** The cluster radius is $R_{\rm SC} = 3$ pc for all these models. Columns 4–7 have the same meaning as in Table 1.

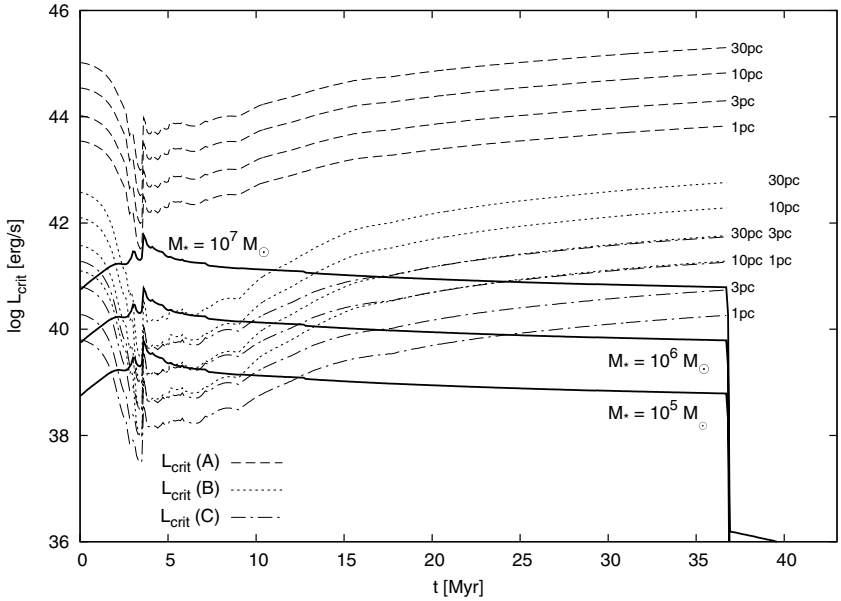


**Figure 7.** Thin lines show the evolution of the critical luminosity, $L_{\rm crit}$, for models A, B, and C (the lines have the same meaning as in Figure 3) and different cluster radii, $R_{\rm SC}$, marked in the figure. Thick solid lines display the mechanical luminosity, $L_{\rm SC}$, for clusters with different stellar masses as denoted in the figure.

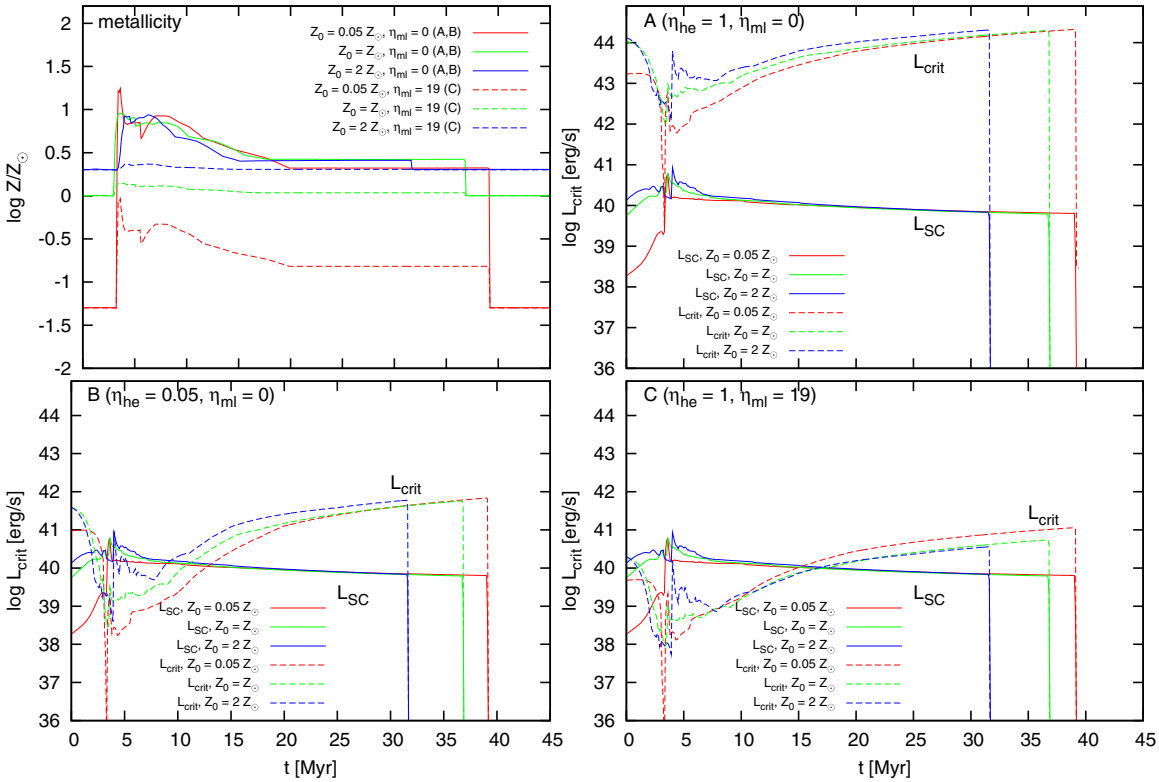


**Figure 8.** Dependence on the stellar metallicity and the metallicity of the mass-loaded gas, $Z_0$. Top left panel shows the metallicity of the supplied gas, $Z$, for models with $\eta_{ml} = 0$ (solid, models A and B) and $\eta_{ml} = 19$ (dashed, model C). Other panels compare the evolution of $L_{SC}$ and $L_{crit}$ with different $Z_0$ for model A (top right), model B (bottom left), and model C (bottom right). In all panels, colors (in the b&w version thickness) of curves represent $Z_0$: $Z_0 = 0.05\ Z_\odot$ (red/thick), $Z_0 = Z_\odot$ (green/medium), and $Z_0 = 2.0\ Z_\odot$ (blue/thin).

(A color version of this figure is available in the online journal.)

**Table 3**
Clusters with Different Radius, $R_{SC}$, Heating Efficiency, $\eta_{he}$, and Mass Loading $\eta_{ml}$

| $R_{SC}$ (pc) | $\eta_{he}$ | $\eta_{ml}$ | $t_{bs}$ (Myr) | $t_{be}$ (Myr) | $M_{acc}$ ($M_\odot$) | $M_{in}$ ($M_\odot$) |
|---|---|---|---|---|---|---|
| 1 | 1 | 0 | ... | ... | 0 | $1.8 \times 10^5$ |
| 3 | 1 | 0 | ... | ... | 0 | $1.8 \times 10^5$ |
| 10 | 1 | 0 | ... | ... | 0 | $1.8 \times 10^5$ |
| 30 | 1 | 0 | ... | ... | 0 | $1.8 \times 10^5$ |
| 1 | 0.05 | 0 | 2.1 | 13.4 | $8.0 \times 10^4$ | $1.8 \times 10^5$ |
| 3 | 0.05 | 0 | 2.4 | 11.1 | $5.8 \times 10^4$ | $1.8 \times 10^5$ |
| 10 | 0.05 | 0 | 2.8 | 9.2 | $3.1 \times 10^4$ | $1.8 \times 10^5$ |
| 30 | 0.05 | 0 | 3.1 | 5.1 | $1.1 \times 10^4$ | $1.8 \times 10^5$ |
| 1 | 1 | 19 | 0.2 | 24.2 | $2.3 \times 10^6$ | $3.7 \times 10^6$ |
| 3 | 1 | 19 | 1.2 | 16.9 | $1.8 \times 10^6$ | $3.7 \times 10^6$ |
| 10 | 1 | 19 | 1.8 | 12.4 | $1.3 \times 10^6$ | $3.7 \times 10^6$ |
| 30 | 1 | 19 | 2.1 | 9.8 | $8.0 \times 10^5$ | $3.7 \times 10^6$ |

**Notes.** The cluster stellar mass is $M_\star = 10^6\ M_\odot$ for all these models. Columns 4–7 have the same meaning as in Table 1.

in the bimodal regime if $M_\star > M_{crit}$. This linear dependence may be broken if the cluster IMF varies with the cluster mass, or if more massive clusters are formed in a different, more abrupt process compared to low-mass clusters. However, in this paper we explore the consequences of an abrupt cluster formation with a given IMF. A discussion of their dependence on the cluster mass exceeds the scope of this paper. The results of the calculations for clusters with different masses and radii in the case when the inserted gas metallicity is solar are summarized in Tables 2 and 3. The tables show that even in the case of low heating efficiency or large mass loading, clusters evolve in the bimodal regime only for some time, as was suggested in Silich et al. (2009). The length of the period of bimodality and the amount of accumulated mass are larger for clusters with smaller radii and larger masses.

Another parameter which may affect properties of the star cluster driven outflows is the re-inserted gas metallicity. In the case of instantaneous star formation, the metallicity of the re-inserted matter changes a lot, as is shown in Figure 2. This should change the cooling rate and thus the critical mechanical luminosity, $L_{crit}$, significantly (Tenorio-Tagle et al. 2005). In order to explore how our results depend on this parameter, we have varied the initial stellar and the loaded gas metallicity, $Z_0$, in our reference models A, B, and C. Three different values of $Z_0$ were used for the calculations: $Z_0 = 0.05\ Z_\odot$, $Z_0 = Z_\odot$, and $Z_0 = 2.0\ Z_\odot$ (see Table 4). The top left panel in Figure 8 shows the trends of the wind metallicity, $Z$, calculated from Equation (7). In all cases without mass loading (solid lines in Figure 8) the metallicity of the thermalized plasma grows rapidly after the first SN explodes, reaches about 10 times the solar value, and then decreases gradually reaching about three times the solar value after ~20 Myr. In the case with mass loading, the maximum metallicity never reaches 10 times the solar value. This is because in this case the re-inserted matter mixes continuously with a large amount of the ablated gas. The calculated critical luminosities, $L_{crit}$, are then compared with the star cluster mechanical luminosities, $L_{SC}$ (top right, bottom left, and bottom right panels in Figure 8 for cases A, B, and C, respectively). Models without mass loading and $\eta_{he} = 1$

**Table 4**
Models with Different Stellar Metallicity, $Z_0$, Heating Efficiency, $\eta_{he}$, and Mass Loading $\eta_{ml}$

| $Z_0$ ($Z_\odot$) | $\eta_{he}$ | $\eta_{ml}$ | $t_{bs}$ (Myr) | $t_{be}$ (Myr) | $M_{acc}$ ($M_\odot$) | $M_{in}$ ($M_\odot$) |
|---|---|---|---|---|---|---|
| 0.05 | 1 | 0 | ... | ... | 0 | $1.8 \times 10^5$ |
| 1.0 | 1 | 0 | ... | ... | 0 | $1.8 \times 10^5$ |
| 2.0 | 1 | 0 | ... | ... | 0 | $1.8 \times 10^5$ |
| 0.05 | 0.05 | 0 | 3.1 | 12.9 | $7.5 \times 10^4$ | $1.8 \times 10^5$ |
| 1.0 | 0.05 | 0 | 2.4 | 11.1 | $5.8 \times 10^4$ | $1.8 \times 10^5$ |
| 2.0 | 0.05 | 0 | 1.9 | 9.3 | $3.7 \times 10^4$ | $1.8 \times 10^5$ |
| 0.05 | 1 | 19 | 2.8 | 15.0 | $1.6 \times 10^6$ | $3.6 \times 10^6$ |
| 1.0 | 1 | 19 | 1.2 | 16.9 | $1.8 \times 10^6$ | $3.7 \times 10^6$ |
| 2.0 | 1 | 19 | 0.4 | 17.0 | $1.8 \times 10^6$ | $3.6 \times 10^6$ |

**Notes.** Other cluster parameters are $R_{SC} = 3$ pc and $M_\star = 10^6\ M_\odot$. Columns 4–7 have the same meaning as in Table 1.

never enter the bimodal regime (see top right panel). Note that relative abundances of species in the re-inserted matter differ from solar values. This implies that the cooling function using scaled solar composition $Z$ may give somewhat different cooling rates than calculated from individual species separately. This, however, does not change our results significantly, since the main coolants (C and O) are also dominant ingredients of $Z$.

## 4. CONCLUSIONS

We used our semi-analytic spherically symmetric code together with the stellar population synthesis model Starburst99 to study the time evolution of SSC winds.

Two physical processes which could affect the hydrodynamics of the star cluster winds significantly and cannot be studied in the semi-analytic approach in detail, the heating efficiency and mass loading, are parameterized with two constant parameters $\eta_{he}$ and $\eta_{ml}$. We also determine how our major results depend on the metallicity of the re-inserted matter.

The calculations show that strong radiative cooling becomes a crucial issue when the wind is mass loaded or the thermalization efficiency (and thus the fraction of the star cluster mechanical luminosity which drives the outflow) is small. In these cases (our reference models C and B, respectively) the evolutionary tracks of the star cluster winds show periods of bimodality. During these periods only some fraction of the re-inserted and loaded gas leaves the cluster as a wind. The rest of the re-inserted matter cools down rapidly, becomes thermally unstable, and is accumulated in the central region of the cluster. The duration of these periods depends on the star cluster parameters $\eta_{he}$ and $\eta_{ml}$. Periods of bimodality are longer in the case of more massive clusters with smaller radii. However, they become progressively shorter as the mass loading drops or the heating efficiency grows. The bimodal regime vanishes in the cases when heating efficiency is large and mass loading is insignificant. In the simulations which include mass loading, the stellar metallicity does not affect significantly either the duration of the bimodal regime or the amount of re-inserted mass which accumulates inside the cluster. Models with low heating efficiency are more sensitive to the metallicity of the re-inserted matter.

We conclude that the second stellar generation may be formed in massive and compact stellar clusters from thermally unstable parts of stellar winds and the mass-loaded gas in their central parts. Low heating efficiency $\eta_{he} = 0.05$ leads to the second stellar generation heavily enriched with He-burning products. However, its total mass is a few percent of the first generation only. A high value of mass loading $\eta_{ml} = 19$ results in the massive second stellar generation; however, its metallicity is only slightly higher than that of the first generation.

We thank our anonymous referee for valuable comments and suggestions. We thank James E. Dale for careful reading of the text and his useful suggestions. This study has been supported by CONACYT-México, research grants 60333 and 131913, and the Spanish Ministry of Science and Innovation under the collaboration ESTALLIDOS (grant AYA2010-21887-C04-04) and Consolider-Ingenio 2010 Program grant CSD2006-00070: First Science with the GTC. R.W. and J.P. acknowledge support from the Institutional Research Plan AV0Z10030501 of the Academy of Sciences of the Czech Republic and project LC06014 Centre for Theoretical Astrophysics of the Ministry of Education, Youth and Sports of the Czech Republic.

## REFERENCES

Bacciotti, F., Hirth, G. A., & Natta, A. 1996, A&A, 310, 309
Beck, S. C. 2008, A&A, 489, 567
Cantó, J., Raga, A. C., & Rodríguez, L. F. 2000, ApJ, 536, 896
Chevalier, R. A., & Clegg, A. W. 1985, Nature, 317, 44
Galliano, E., Alloin, D., Pantin, E., et al. 2008, A&A, 492, 3
Gilbert, A. M., & Graham, J. R. 2007, ApJ, 668, 168
Henry, A. L., Turner, J. L., Beck, S. C., Crosthwaite, L. P., & Meier, D. S. 2007, AJ, 133, 757
Holtzman, J. A., Faber, S. M., Shaya, E. J., et al. 1992, AJ, 103, 691
Kroupa, P. 2001, MNRAS, 322, 231
Leitherer, C., Robert, C., & Drissen, L. 1992, ApJ, 401, 596
Leitherer, C., Schaerer, D., Goldader, J. D., et al. 1999, ApJS, 123, 3
Melioli, C., & de Gouveia Dal Pino, E. M. 2004, A&A, 424, 817
Melo, V. P., Muñoz-Tuñón, C., Maíz-Apellániz, J., & Tenorio-Tagle, G. 2005, ApJ, 619, 270
O'Connell, R. W., Gallagher, J. S., III, Hunter, D. A., & Colley, W. N. 1995, ApJ, 446, L1
Plewa, T. 1995, MNRAS, 275, 143
Raga, A. C., Velázquez, P. F., Cantó, J., Masciadri, E., & Rodríguez, L. F. 2001, ApJ, 559, L33
Silich, S., Tenorio-Tagle, G., & Muñoz-Tuñón, C. 2003, ApJ, 590, 791
Silich, S., Tenorio-Tagle, G., & Muñoz-Tuñón, C. 2007, ApJ, 669, 952
Silich, S., Tenorio-Tagle, G., Muñoz-Tuñón, C., et al. 2010, ApJ, 711, 25
Silich, S., Tenorio-Tagle, G., & Rodríguez-González, A. 2004, ApJ, 610, 226
Silich, S., Tenorio-Tagle, G., Torres-Campos, A., et al. 2009, ApJ, 700, 931
Smith, L. J., Westmoquette, M. S., Gallagher, J. S., et al. 2006, MNRAS, 370, 513
Stevens, I. R., & Hartwell, J. M. 2003, MNRAS, 339, 280
Tenorio-Tagle, G., Muñoz-Tuñón, C., Pérez, E., Silich, S., & Telles, E. 2006, ApJ, 643, 186
Tenorio-Tagle, G., Silich, S., Rodríguez-González, A., & Muñoz-Tuñón, C. 2005, ApJ, 628, L13
Tenorio-Tagle, G., Wünsch, R., Silich, S., Muñoz-Tuñón, C., & Palouš, J. 2010, ApJ, 708, 1621
Tenorio-Tagle, G., Wünsch, R., Silich, S., & Palouš, J. 2007, ApJ, 658, 1196
Whelan, D. G., Johnson, K. E., Whitney, B. A., Indebetouw, R., & Wood, K. 2011, ApJ, 729, 111
Whitmore, B. C., Schweizer, F., Leitherer, C., Borne, K., & Robert, C. 1993, AJ, 106, 1354
Wünsch, R., Silich, S., Palouš, J., & Tenorio-Tagle, G. 2007, A&A, 471, 579
Wünsch, R., Tenorio-Tagle, G., Palouš, J., & Silich, S. 2008, ApJ, 683, 683